Infrared spectroscopy of hole-doped ABA-stacked trilayer graphene

Infrared spectroscopy of hole-doped ABA-stacked trilayer graphene

N. Ubrig[1], P. Blake[2], D. van der Marel[1] and A. B. Kuzmenko[1(a)]

[1] *Département de Physique de la Matière Condensée, Université de Genève - CH-1211 Genève 4, Switzerland*
[2] *Graphene Industries Ltd, Manchester Centre for Mesoscience and Nanotechnology, University of Manchester*
Manchester, M13 9PL, UK, EU

Abstract – Using infrared spectroscopy, we investigate bottom gated ABA-stacked trilayer graphene subject to an additional environment-induced p-type doping. We find that the Slonczewski-Weiss-McClure tight-binding model and the Kubo formula reproduce the gate voltage-modulated reflectivity spectra very accurately. This allows us to determine the charge densities and the potentials of the π-band electrons on all graphene layers separately and to extract the interlayer permittivity due to higher-energy bands.

Introduction. – Trilayer graphene has recently attracted much interest because its electronic structure is distinctly different from the bands found in more studied monolayer and bilayer graphene. Interestingly, the two major stacking types of trilayer graphene, namely the Bernal (or ABA-) stacking and the rhombohedral (ABC-) stacking, result in rather different band properties [1]. In rhombohedral graphene, a sizeable bandgap can be generated and tuned with an external electric field [2–5], while in Bernal stacked graphene the dominant effect is gate-tunable band overlap [2,6–11], resulting in a semimetallic behaviour. Trilayer graphene presents the simplest case where the complete set of Slonczewski-Weiss-McClure (SWM) tight-binding parameters is needed to describe the band structure, as it is the case for three-dimensional graphite [12,13]. However, in contrast to graphite, trilayer graphene allows exploring different doping regimes and the effect of an electric field on the band structure. Thus, it might be beneficial for understanding the complex graphite physics to study its trilayer counterpart.

In this work we focus on the ABA-stacked trilayer graphene, the form most often found in nature, which is plane symmetric with respect to the middle layer. Our goal is to determine experimentally optical properties as a function of an external electric field and check the ability of the existing theories to reproduce them quantitatively. The sample is a bottom gated exfoliated flake. Its charge neutrality point is strongly shifted with respect to zero gate voltage, which allows us to explore the high-doping regime not achieved so far in a combination with infrared spectroscopy. By treating the electrostatic potentials of each of the three layers as gate voltage-dependent free parameters, we achieve a very good match between the experiment and the tight-binding model. With the help of a basic electrostatic model for trilayer graphene [7,8] we find an accurate value for the static perpendicular inter-plane permittivity ε_r due to the cumulative polarizability of all electronic shells except the low-energy π-bands, considered explicitly by the tight-binding model.

Experimental results. – A large, several tens of micrometers, flake of trilayer graphene was obtained by mechanical exfoliation [14] and deposited on a Si substrate covered by a 300 nm layer of silicon oxide (fig. 1(a)). Electrical contacts were deposited by evaporating gold through a shadow mask. The stacking was identified as of ABA type, based on Raman spectroscopy [15] and infrared spectroscopy as discussed below.

The resistivity curve (fig. 1(b)) shows that the sample is strongly hole doped so that the charge neutrality point cannot be achieved even by applying $V_g = +80\,\mathrm{V}$ to the gate. Annealing the sample several times at $200\,^\circ\mathrm{C}$ in a H_2-N_2 atmosphere did not change significantly the resistivity curve. We therefore attribute the extrinsic doping either to gold atoms, generally known to dope graphene positively [16,17], scattered below the shadow mask onto
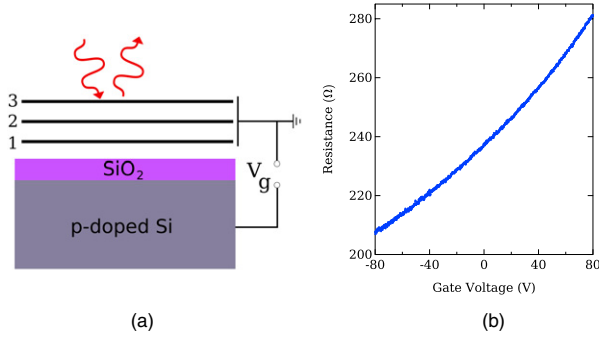
Fig. 1: (a) (Color online) Schematic representation of bottom gated three-layer graphene used in this study. The layer numbering used in the text is given. (b) The resistance of the sample as a function of the gate voltage at 20 K.
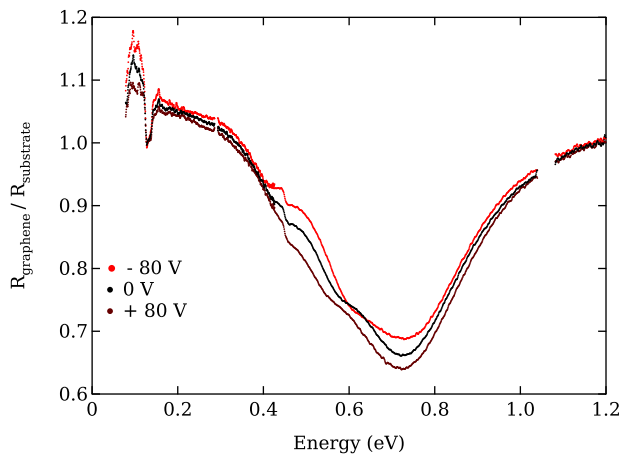

Fig. 2: (Color online) Reflectivity of trilayer graphene at 20 K for different gate voltages of −80, 0 and +80 V.
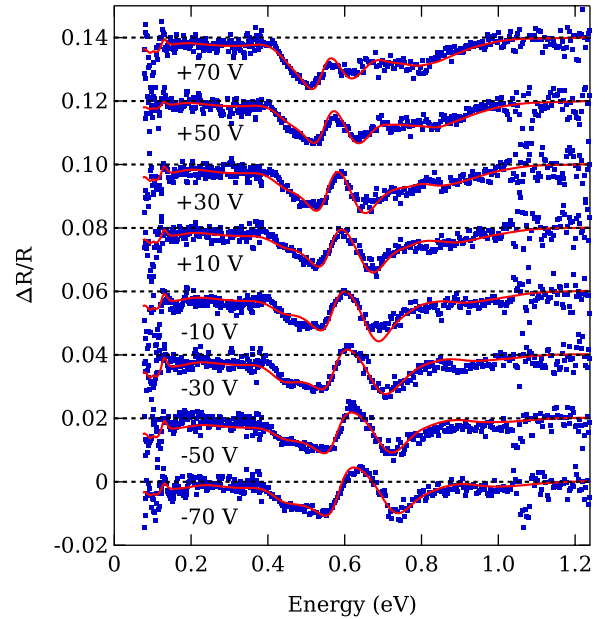

Fig. 3: (Color online) Experimental differential reflectivity for pairs of consecutive gate voltages. The value given for each curve is the average of the two voltages (separated by 20 V) used to generate the difference. For clarity each curve is shifted and the zero levels are indicated by dotted lines. The points represent the experimental data, while the solid red line is the result of the fit.

the graphene surface during the contact evaporation or to a layer of water or hydrocarbon contamination trapped below the flake [18]. Although not being able to reach the electron-type doping, we benefited from this situation by measuring in the regime of high hole doping $(\sim 3 \cdot 10^{13}\,\mathrm{cm}^{-2})$, which would not be achievable with an initially undoped sample.

The reflectivity measurements at various gate voltages between −80 V and +80 V with a step of 20 V were performed at 20 K in a helium-flow cryostat mounted on an infrared microscope coupled to a Fourier transform infrared spectrometer. The infrared spot of about 15 × 15 μm was kept far from the flake edges and electrical contacts. Each measurement on graphene was followed by recording reference spectra on the bare substrate and on gold. A black-body Globar light source was used between 0.1 and 0.7 eV and a tungsten lamp was employed between 0.4 and 1.5 eV.

The reflectivity of trilayer graphene normalized by the bare substrate is plotted in fig. 2 for gate voltages of −80, 0 and +80 V. Although the changes between the spectra are caused by the modification of the optical properties of graphene, some profound spectral features present in all spectra are due to the substrate. For example, the strong structure at about 0.1 eV is due to optical phonons in SiO$_2$. The deep minimum at 0.7 eV, where the presence of graphene reduces the reflected signal by almost 40 percent, is due to the Fabry-Pérot interference in the oxide layer.

Even though the substrate somewhat complicates the interpretation of the measured spectra, some qualitative observations can be made without data modeling. First, at energies below about 1 eV the reflectivity systematically decreases as the gate voltage increases. This is directly related to the decreasing metallicity and Drude weight as the concentration of holes is reduced. Second, above 1 eV the curves essentially overlay showing that the electric field has little or no influence on the optical properties at high energies. Third, in the region between about 0.4 and 0.8 eV, a more complex gate voltage dependence is observed, which is due to interband transitions in graphene.

In order to emphasize the effect of the gate and to extract more information from the data, we show in fig. 3 the differential (or contrast) spectra for all pairs of consecutive gate voltages. They are defined as follows [19]:

$$\frac{\Delta R}{R}(\omega, V_g) = 2\frac{R(\omega, V_g + 10V) - R(\omega, V_g - 10V)}{R(\omega, V_g + 10V) + R(\omega, V_g - 10V)}. \quad (1)$$

The curves are marked by pronounced spectral structures showing a strong gate dependence. For example, the
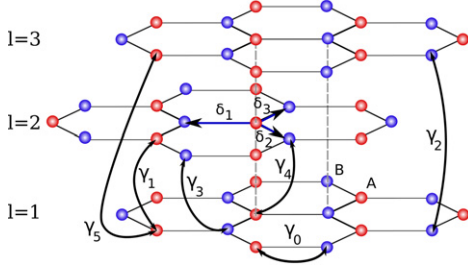
Fig. 4: (Color online) The crystal lattice of ABA-stacked trilayer graphene with the definition of the hopping parameters.

position of the peak at around $0.6\,\mathrm{eV}$ shifts by almost $0.1\,\mathrm{eV}$ as the gate voltage is swept from $+70\,\mathrm{V}$ to $-70\,\mathrm{V}$. The shape of the structures is also strongly influenced by the gate. Such a non-trivial behavior of the contrast spectra is due to the fact that not only the chemical potential is modified by the gate voltage but also the band structure is affected by the gate-induced electric field. Thus, quantitative modeling is required in order to identify spectral features and to get further insight into the effect of the gate on the electronic structure of the sample. Below we discuss this analysis in detail. Looking ahead, we note here that a very good agreement between the data and the tight-binding model of the ABA-stacked graphene is achieved (red solid lines in fig. 3). Given that the band structures of ABC- and ABA-stacked graphene are entirely different [1], we conclude that the sample is ABA-stacked.

Optical-data modeling. – To model the optical data we use a tight-binding description of trilayer graphene [7,8] based on the SWM-model of graphite [12,13]. The hopping terms γ_0, γ_1, γ_2, γ_3, γ_4 and γ_5 are illustrated in fig. 4. Additionally, Δ represents the difference between the on-site energy for the two sublattices A and B (marked with red and blue colors, respectively). To account for the effect of an external electric field we add potentials U_1, U_2 and U_3 to the first, second and the third layers, respectively [7]. In the basis of $|A_1\rangle$, $|B_1\rangle$, $|A_2\rangle$, $|B_2\rangle$, $|A_3\rangle$ and $|B_3\rangle$ the Hamiltonian of ABA-stacked trilayer graphene reads

$$\mathbf{H} = \begin{pmatrix} U_1 & \gamma_0\phi & -\gamma_4\phi & \gamma_3\phi^* & \gamma_2 & 0 \\ \gamma_0\phi^* & U_1+\Delta & \gamma_1 & -\gamma_4\phi & 0 & \gamma_5 \\ -\gamma_4\phi^* & \gamma_1 & U_2+\Delta & \gamma_0\phi & -\gamma_4\phi^* & \gamma_1 \\ \gamma_3\phi & -\gamma_4\phi^* & \gamma_0\phi^* & U_2 & \gamma_3\phi & -\gamma_4\phi^* \\ \gamma_2 & 0 & -\gamma_4\phi & \gamma_3\phi^* & U_3 & \gamma_0\phi \\ 0 & \gamma_5 & \gamma_1 & -\gamma_4\phi & \gamma_0\phi^* & U_3+\Delta \end{pmatrix} \quad (2)$$

with

$$\phi = e^{i\boldsymbol{k}\,\boldsymbol{\delta}_1} + e^{i\boldsymbol{k}\,\boldsymbol{\delta}_2} + e^{i\boldsymbol{k}\,\boldsymbol{\delta}_3} \quad (3)$$

where $\boldsymbol{k}$ is the momentum with respect to the K-point of the Brillouin zone and the vectors $\boldsymbol{\delta}_{1,2,3}$ connect the nearest neighbor atoms as shown in fig. 4.

In order to obtain the optical properties of this system, within the linear response theory, we use the Kubo formula for the optical sheet conductivity $\sigma(\omega)$. We calculate

the Drude and the interband terms using the following expressions:

$$\sigma_D = \frac{2\sigma_0}{\pi} \sum_i \int \mathrm{d}^2\boldsymbol{k} \left| \langle \boldsymbol{k}, i | \frac{\partial \mathbf{H}}{\partial k_x} | \boldsymbol{k}, i \rangle \right|^2$$
$$\cdot \frac{-\partial f(\epsilon_{\boldsymbol{k},i})}{\partial \epsilon} \cdot \frac{i}{\hbar\omega + i\Gamma_D} \quad (4)$$

and

$$\sigma_{IB} = \frac{2\sigma_0}{\pi} \sum_{i,j\neq i} \int \mathrm{d}^2\boldsymbol{k} \left| \langle \boldsymbol{k}, i | \frac{\partial \mathbf{H}}{\partial k_x} | \boldsymbol{k}, j \rangle \right|^2$$
$$\cdot \frac{f(\epsilon_{\boldsymbol{k},i}) - f(\epsilon_{\boldsymbol{k},j})}{\epsilon_{\boldsymbol{k},i} - \epsilon_{\boldsymbol{k},j}} \cdot \frac{i}{\hbar\omega - \epsilon_{\boldsymbol{k},j} + \epsilon_{\boldsymbol{k},i} + i\Gamma}, \quad (5)$$

where $\sigma_0 = e^2/4\hbar \approx 6.08 \cdot 10^{-5}\,\Omega^{-1}$ is the universal AC conductance of monolayer graphene [20], $\epsilon_{\boldsymbol{k},i}$ is the band energy ($i = 1, \ldots, 6$), $f(\epsilon) = (1 + \exp(\frac{\epsilon-\mu}{k_BT}))^{-1}$ is the Fermi-Dirac distribution and μ is the chemical potential. Γ and Γ_D are the electronic broadening parameters for the interband and the intraband transitions, respectively. For simplicity, the interband broadening is taken to be momentum-, energy-, band- and doping-independent.

The total charge density n_{total} and the charge densities of each layer, n_l ($l = 1, 2, 3$), can also be calculated through

$$n_{\mathrm{total}} = \frac{1}{2\pi^2} \sum_i \int \mathrm{d}^2\boldsymbol{k} \left(f(\epsilon_{i,\boldsymbol{k}}) - \frac{1}{2} \right) \quad (6)$$

and

$$n_l = \frac{1}{2\pi^2} \sum_i \int \mathrm{d}^2\boldsymbol{k} \left(f(\epsilon_{i,\boldsymbol{k}}) - \frac{1}{2} \right)$$
$$\cdot \left(|\psi_{A_l}|^2 + |\psi_{B_l}|^2 \right), \quad (7)$$

where we subtract $\frac{1}{2}$ in order to count the doping level with respect to half filling of the π-bands. ψ_{A_l} and ψ_{B_l} are the projections of the total electronic eigenfunction on the sublattices A_l and B_l.

Once the conductivity is determined we can calculate the optical reflectivity of the complete graphene/SiO$_2$/Si system using Fresnel equations and consequently compute the differential reflectivity (eq. (1)). As $\Delta R/R$ values are rather small it is useful to introduce the so-called sensitivity functions [19] $\beta_1(\omega)$, $\beta_2(\omega)$, which are determined by the substrate, and to employ the linearized formula

$$\frac{\Delta R}{R} \approx \beta_1(\omega) \frac{\mathrm{Re}\Delta\sigma(\omega)}{\sigma_0} + \beta_2(\omega) \frac{\mathrm{Im}\Delta\sigma(\omega)}{\sigma_0}. \quad (8)$$

When fitting the experimental data, we fixed the SWM parameters to the values published in ref. [21], which we reproduce in table 1 for the sake of convenience. We also fixed the Drude broadening Γ_D to $5\,\mathrm{meV}$ [22] as its value has almost no influence on the optical data in the studied spectral range. In contrast, the interband broadening Γ strongly affects the data, resulting in the
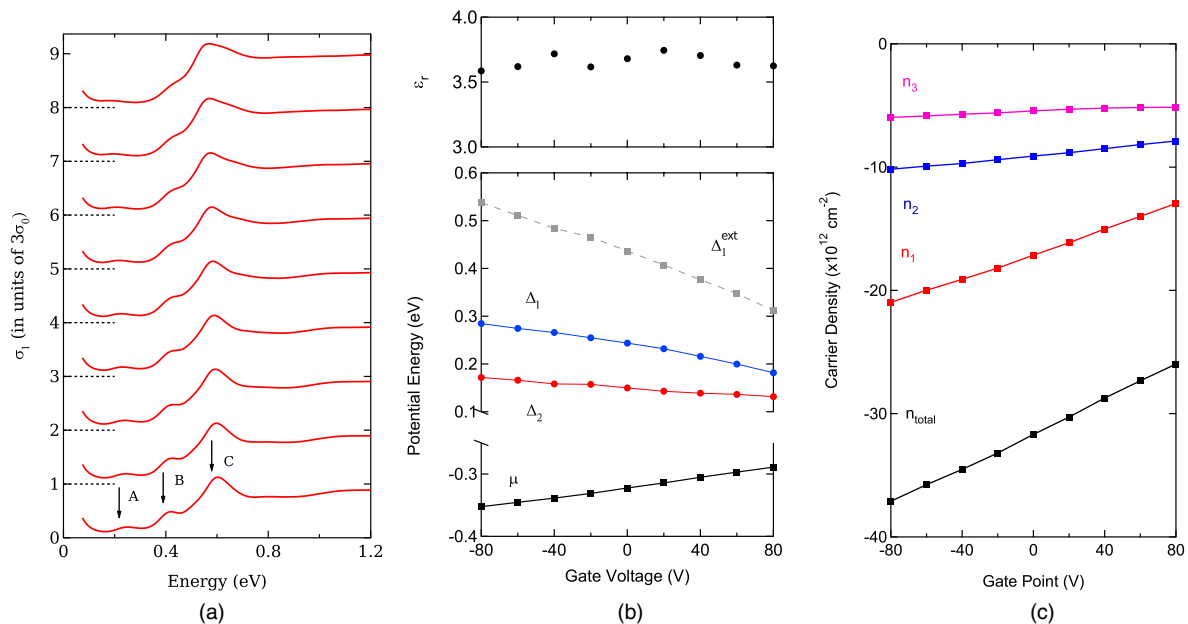
Fig. 5: (a) (Color online) The calculated optical sheet conductivity at different gate voltages obtained from the fits shown in fig. 3 as described in the text. The arrows mark the dominant peaks corresponding to the interband transitions indicated in fig. 6. (b) The interplane potentials Δ_1, Δ_2 and the chemical potential μ as a function of the gate voltage, directly obtained from the optical fits. Also shown are the derived values of the external potential Δ_1^{ext} and the interspace permittivity ε_r. (c) The charge densities n_l of each layer and the total density n_{total} as a function of the gate voltage.

Table 1: SWM band parameters used in this work to fit the optical spectra. The values are taken from ref. [21].

Parameter	Value (eV)
γ_0	3.12
γ_1	0.377
γ_2	-0.0206
γ_3	0.29
γ_4	0.12
γ_5	0.025
Δ	0.0138

overall smoothening of the spectral structures. It was therefore taken as an adjustable parameter, for which the best value was found to be 45 meV.

The most important detail of our fitting procedure is that we treat the chemical potential and the plane potentials U_l as independent adjustable parameters at every value of V_g, in order to extract the actual gate voltage dependence of these quantities from the optical data. It is easy to see that shifting the values of μ, U_1, U_2 and U_3 by the same amount does not change any physical properties such as the optical spectra and the charge density. To remove this ambiguity, we imposed an additional condition, $U_1 + U_2 + U_3 = 0$.

The best fits are shown in fig. 3 with the solid red lines. One can notice an excellent match between the experiment and the model, including all spectral features at all gate voltages. It is worth mentioning that although

the differential reflectivity between 0.15 and 0.4 eV is rather featureless it is distinctly non-zero. This is caused by the gate variable Drude contribution and the model reproduces this fact very well.

As all the curves were fitted *simultaneously*, the obtained parameters were well defined and converged to the same numbers, which we carefully tested by using different fitting procedures and by varying the initial parameter values. The robustness of these results allows us to develop a deeper analysis of the response of graphene to the external electric field which we present in the next section.

Discussion. – The optical conductivity spectra corresponding to the fits described above are shown in fig. 5(a) for each value of the gate voltage. For illustration purposes, the curves are normalized by $3 \cdot \sigma_0$. At low photon energies but above the Drude peak, the optical conductivity is significantly below $3 \cdot \sigma_0$, while at high photon energies it approaches this value. This is related to the Pauli blocking, which results, in the case of monolayer graphene, in a conductivity step at 2μ [23]. Additionally, significant spectral features are the peaks at approximately 0.25 eV, 0.42 eV and 0.6 eV, which are denoted, respectively, as A, B and C in fig. 5(a). They can be assigned to transitions between almost parallel bands, which are illustrated in fig. 6. The energy of the strongest peak (C) is close to $\sqrt{2}\gamma_1$, in agreement with the theoretical predictions [6,24,25] and experimental data [4,11,15,26]. The peaks noticeably shift as a function of the gate voltage. For example, peak C moves from
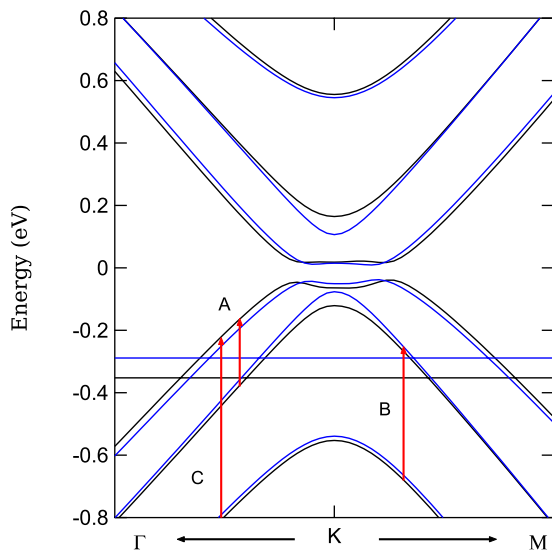
Fig. 6: (Color online) Electronic bands at $V_g = -80\,\text{V}$ (solid black lines) and $+80\,\text{V}$ (dashed blue lines) calculated based on the fits in fig. 3. The horizontal lines indicate the chemical potential. The arrows correspond to the optical peaks indicated in fig. 5(a).

0.55 eV at $V_g = +80\,\text{V}$ to 0.6 eV at $V_g = -80\,\text{V}$. As can be seen in fig. 6, this effect stems from the field-induced displacement of the bands with respect to each other. The transitions are broad because the scattering parameter Γ is large, as compared to the numbers obtained in low doped samples [4]. We believe that extra scattering present here is due to the charged impurities that also give rises to the elevated doping.

Let us now inspect the dependence of the doping and the interplane potentials on the gate voltage. In fig. 5(b) we plot the chemical potential as a function of the applied gate. It is always negative with a high absolute value and moves gradually towards the charge neutrality as the gate voltage is increased. This corroborates our initial observation of a high level of hole doping.

The total charge carrier density n_{total} obtained using eq. (6) is shown in fig. 5(c). At zero voltage the concentration of holes is about $3 \cdot 10^{13}\,\text{cm}^{-2}$. It changes linearly with V_g with a slope dn_{total}/dV_g equal to $7.0 \cdot 10^{10}\,\text{cm}^{-2}\,\text{V}^{-1}$. Remarkably, this value, which is based on the optical data only, agrees extremely well with the expected slope of $7.2 \cdot 10^{10}\,\text{cm}^{-2}\,\text{V}^{-1}$ for the actual thickness of the oxide layer [14], thus providing extra credence to our analysis. From this dependence, one expects to reach the charge neutrality point at $V_g \approx +450\,\text{V}$, which is not achievable in the present experiment.

In the same figure, we present the charge density on each layer separately according to eq. (7). As expected, the layer closest to the gate shows the strongest charge variation as a function of the external field, while the effect of the gate decreases strongly with increasing layer index due to internal screening. This is in good agreement with theoretical predictions [8].

In fig. 5(b) we plot the potential difference between the outer layers, $\Delta_1 = U_1 - U_3$, and twice the difference between the average of the potentials of outer layers and the one of the central layer, $\Delta_2 = U_1 + U_3 - 2U_2$, introduced in ref. [7]. These parameters fully characterize the distribution of the potential in the sample. We first note that the value of Δ_1 is not zero but 0.25 eV in the absence of the gate voltage. Such a large potential asymmetry can be attributed to environmental impurities in contact with the sample, whose charging effect is not symmetrical with respect to the graphene plane. Since Δ_1 depends on V_g, the gate also contributes to the total electric field across the sample. The physical meaning of the parameter Δ_2, which is also finite at $V_g = 0$ and shows a noticeable gate voltage dependence, will become clear in the following.

Within a simple electrostatic model [7,8,27] where each graphene layer is treated as an infinitely thin charged plane the electrostatic potentials can be straightforwardly related to the charge densities:

$$\Delta_1 = \frac{e^2 d}{\varepsilon_0 \varepsilon_r}(n_1 - n_3) + \Delta_1^{\text{ext}}, \qquad (9)$$

and

$$\Delta_2 = -\frac{e^2 d}{\varepsilon_0 \varepsilon_r} n_2, \qquad (10)$$

where e is the elementary charge, ε_0 the vacuum permittivity, $d \approx 0.335\,\text{nm}$ the interlayer distance and ε_r the interplane permittivity between graphene layers due to the screening effect of all electrons except the π-band electrons. The quantity Δ_1^{ext} takes into account the effect of the gate voltage and the environmental charges, which would produce a potential difference exactly equal to Δ_1^{ext} over the distance of $2d$ in the absence of electrostatic screening by graphene.

Interestingly, all the quantities that enter eq. (10), except ε_r, are known from the infrared data, which allows us to derive the interplane permittivity. From fig. 5(b) we cannot identify any dependence of ε_r on the gate voltage, and its value is 3.7 ± 0.1.

To our knowledge, there are no direct measurements of this quantity, which is however an important parameter needed to calculate the electronic screening in graphene. One should note that no relation analogous to eq. (10) exists in the case of bilayer graphene allowing such a straightforward determination of ε_r. It turns out that the high doping level of our sample is beneficial for the accuracy of this method since ε_r is proportional to the ratio of n_2 and Δ_2, which would both be very small in an undoped sample.

Once the value of ε_r is determined, we can calculate Δ_1^{ext} with eq. (9) for each gate voltage (light gray squares in fig. 5(b)). Δ_1^{ext} decreases linearly as a function of V_g with a slope of about $-0.0014\,\text{eV/V}$. Within the same electrostatic model, the slope is expected to be $d\Delta_1^{\text{ext}}/dV_g = -(de\varepsilon_r) \cdot (\varepsilon_b/L_b) = -0.0012\,\text{eV/V}$, where

$\varepsilon_b = 3.9$ and $L_b = 300\,$nm are the dielectric constant and the thickness of the oxide layer, respectively. The experimental and the theoretical values are thus very close, supporting the model.

It is interesting to follow the modification of the band structure by the gate voltage. The bands corresponding to the best fits of the optical spectra are displayed for $V_g = -80\,$V and $V_g = +80\,$V in fig. 6. Although the bands for the presented voltages are qualitatively similar, their positions and shapes, especially near the K-point, are significantly influenced by the electric field. In both cases, there is a gap of about 50 meV between the valence and the conduction bands. However, the chemical potential does not lie inside the gap, giving rise to a metallic, rather than semiconducting electronic properties. Notably in our highly doped sample the gap is much larger than the prediction for weakly doped ABA-stacked trilayers [8,28,29].

In conclusion, we investigated highly p-type doped ABA-stacked trilayer graphene with infrared spectroscopy. By fitting the experimental reflectivity spectra with a tight-binding model and the Kubo formula we extract the intrinsic parameters such as the carrier density and potentials of individual graphene layers. With a simple electrostatic model we can account for the effect of environmental charging and determine the interlayer permittivity between two graphene layers due to all the electronic shells except the π-bands. We show that, due to a large potential difference across the layers, a sizeable band gap in ABA-trilayer graphene is induced. Our work demonstrates new abilities of infrared spectroscopy in studying electronic screening in graphene multilayers.

$$* * *$$

REFERENCES

[1] Guinea F., Castro Neto A. H. and Peres N. M. R., *Phys. Rev. B*, **73** (2006) 245426.
[2] Aoki M. and Amawashi H., *Solid State Commun.*, **142** (2007) 123.
[3] Zhang F., Sahu B., Min H. and MacDonald A. H., *Phys. Rev. B*, **82** (2010) 035409.
[4] Lui C. H., Li Z., Mak K. F., Cappelluti E. and Heinz T. F., *Nat. Phys.*, **7** (2011) 944.
[5] Avetisyan A. A., Partoens B. and Peeters F. M., *Phys. Rev. B*, **81** (2010) 115432.
[6] Lu C. L., Chang C. P., Huang Y. C., Chen R. B. and Lin M. L., *Phys. Rev. B*, **73** (2006) 144427.
[7] Koshino M. and McCann E., *Phys. Rev. B*, **79** (2009) 125443.
[8] Avetisyan A. A., Partoens B. and Peeters F. M., *Phys. Rev. B*, **79** (2009) 035421.
[9] Craciun M. F., Russo S., Yamamoto M., Oostinga J. B., Morpurgo A. F. and Tarucha S., *Nat. Nanotechnol.*, **4** (2009) 383.
[10] Bao W., Jing J. V. L. jr., Lee Y., Liu G., Tran D., Standley B., Aykol M., Cronin S. B., Smirnov D. *et al.*, *Nat. Phys.*, **7** (2011) 948.
[11] Henriksen E. A., Nandi D. and Eisenstein J. P., *Phys. Rev. X*, **2** (2012) 011004.
[12] McClure J. W., *Phys. Rev.*, **108** (1957) 612.
[13] Slonczewski J. C. and Weiss P. R., *Phys. Rev.*, **109** (1958) 272.
[14] Novoselov K. S., Jiang D., Schedin F., Booth T. J., Khotkevich V. V., Morozov S. V. and Geim A. K., *Proc. Natl. Acad. Sci. U.S.A.*, **102** (2005) 10451.
[15] Lui C. H., Li Z., Chen Z., Klimov P. V., Brus L. E. and Heinz T. F., *Nano Lett.*, **11** (2010) 164.
[16] Gierz I., Riedl C., Starke U., Ast C. R. and Kern K., *Nano Lett.*, **8** (2008) 4603.
[17] Klusek Z., Dabrowski P., Kowalczyk P., Kozlowski W., Olejniczak W., Blake P., Szybowicz M. and Runka T., *Appl. Phys. Lett.*, **95** (2009) 113114.
[18] Haigh S. J., Gholinia A., Jalil R., Romani S., Britnell L., Elias D. C., Novoselov K. S., Ponomarenko L. A., Geim A. K. and Gorbachev R., *Nat. Mater.*, **11** (2012) 764, doi:10.1038/nmat3386.
[19] Kuzmenko A. B., Crassee I., van der Marel D., Blake P. and Novoselov K. S., *Phys. Rev. B*, **80** (2009) 165406.
[20] Ando T., Zheng Y. and Suzuura H., *J. Phys. Soc. Jpn.*, **71** (2002) 1318.
[21] Partoens B. and Peeters F. M., *Phys. Rev. B*, **74** (2006) 075404.
[22] Kuzmenko A. B., van Heumen E., Carbone F. and van der Marel D., *Phys. Rev. Lett.*, **100** (2008) 117401.
[23] Li Z. Q., Henriksen E. A., Jiang Z., Hao Z., Martin M. C., Kim P., Stormer H. L. and Basov D. N., *Nat. Phys.*, **4** (2008) 532.
[24] Koshino M. and Ando T., *Phys. Rev. B*, **77** (2008) 115313.
[25] Koshino M. and Ando T., *Solid State Commun.*, **149** (2009) 1123.
[26] Mak K. F., Sfeir M. Y., Misewich J. A. and Heinz T. F., *Proc. Natl. Acad. Sci. U.S.A*, **107** (2010) 14999.
[27] McCann E. and Koshino M., arXiv:1205.6953 (2012).
[28] Wu B., *Appl. Phys. Lett.*, **98** (2011) 263107.
[29] Avetisyan A. A., Partoens B. and Peeters F. M., *Phys. Rev. B*, **80** (2009) 195401.